




Article

Bis-thiobarbiturates as Promising Xanthine Oxidase Inhibitors: Synthesis and Biological Evaluation

João L. Serrano ¹, Diana Lopes ¹, Melani J. A. Reis ¹, Renato E. F. Boto ¹, Samuel Silvestre ^{1,2,*}
and Paulo Almeida ^{1,*}

¹ CICS-UBI—Health Sciences Research Center, University of Beira Interior, Av. Infante D. Henrique, 6200-506 Covilhã, Portugal; joao.serrano@ubi.pt (J.L.S.); nekolopes@hotmail.com (D.L.); joanareis_95@hotmail.com (M.J.A.R.); rboto@ubi.pt (R.E.F.B.)

² CNC—Center for Neuroscience and Cell Biology, University of Coimbra, Rua Larga, 3004-517 Coimbra, Portugal

* Correspondence: sms@ubi.pt (S.S.); paulo.almeida@ubi.pt (P.A.)

Abstract: Xanthine oxidase (XO) is the enzyme responsible for the conversion of endogenous purines into uric acid. Therefore, this enzyme has been associated with pathological conditions caused by hyperuricemia, such as the disease commonly known as gout. Barbiturates and their congeners thiobarbiturates represent a class of heterocyclic drugs capable of influencing neurotransmission. However, in recent years a very large group of potential pharmaceutical and medicinal applications have been related to their structure. This great diversity of biological activities is directly linked to the enormous opportunities found for chemical change off the back of these findings. With this in mind, sixteen bis-thiobarbiturates were synthesized in moderate to excellent reactional yields, and their antioxidant, anti-proliferative, and XO inhibitory activity were evaluated. In general, all bis-thiobarbiturates present a good antioxidant performance and an excellent ability to inhibit XO at a concentration of 30 μM , eight of them are superior to those observed with the reference drug allopurinol (Allo), nevertheless they were not as effective as febuxostat. The most powerful bis-thiobarbiturate within this set showed in vitro IC_{50} of 1.79 μM , which was about ten-fold better than Allo inhibition, together with suitable low cytotoxicity. In silico molecular properties such as drug-likeness, pharmacokinetics, and toxicity of this promising barbiturate were also analyzed and herein discussed.

Keywords: bis-thiobarbiturates; xanthine oxidase; antioxidant; cytotoxicity; in silico evaluation



Citation: Serrano, J.L.; Lopes, D.; Reis, M.J.A.; Boto, R.E.F.; Silvestre, S.; Almeida, P. Bis-thiobarbiturates as Promising Xanthine Oxidase Inhibitors: Synthesis and Biological Evaluation. *Biomedicines* **2021**, *9*, 1443. <https://doi.org/10.3390/biomedicines9101443>

Academic Editor: Maria Stefania Sinicropi

Received: 14 September 2021

Accepted: 8 October 2021

Published: 11 October 2021

Publisher's Note: MDPI stays neutral with regard to jurisdictional claims in published maps and institutional affiliations.



Copyright: © 2021 by the authors. Licensee MDPI, Basel, Switzerland. This article is an open access article distributed under the terms and conditions of the Creative Commons Attribution (CC BY) license (<https://creativecommons.org/licenses/by/4.0/>).

1. Introduction

Xanthine oxidase (XO) is a molybdoflavoprotein widely disseminated throughout the human body, and is present in the liver, intestine, lungs, kidneys, heart, brain, and plasma [1]. Physiologically, XO catalyzes the oxidative hydroxylation of hypoxanthine and xanthine into uric acid (UA) with the concomitant production of reactive oxygen species (ROS) [1]. Therefore, this enzyme is an important source of superoxide radicals and hydrogen peroxide, which contributes to oxidative stress and takes part in the aging process. In addition, these ROS are involved in several pathological processes such as atherosclerosis and cancer [2,3]. Moreover, the excessive activity of XO leads to the overproduction of UA, increasing its concentration in the bloodstream and can result in hyperuricemia [4]. Hyperuricemia is a predisposing factor of gout, whether by excessive production of UA or under-excretion by the kidneys and is also considered a lifestyle-related syndrome. In fact, it has been associated with a high intake of foods rich in nucleic acids, such as red meats and seafood, leading to excessive production of UA [5,6].

Gout is a form of inflammatory arthritis characterized by the chronic deposition of monosodium urate crystals on the joints [4,6]. Hyperuricemia is a critical factor, not only for the development of gout but also for chronic nephritis, cardiovascular diseases,

hypertension, type II diabetes mellitus, and metabolic syndrome [6]. The standard therapy for gout relies on urate-lowering drugs, especially those that target XO [4,6], such as allopurinol (Allo), febuxostat, and topiroxostat [1,6–8].

The synthesis and biological evaluation of nitrogen-based heterocyclic compounds has received increasing attention over the years [9]. Barbituric and thiobarbituric acids are examples of these heterocycles. Firstly synthesized by Adolph von Baeyer in 1864, barbituric acid was the key molecule for developing new derivatives with central nervous system (CNS) depressing activity in the twentieth century [10]. Initially used as anticonvulsant, anxiolytic, sedative-hypnotic and anesthetics [10], barbituric and thiobarbituric acid derivatives have recently been associated with several potential industrial and pharmaceutical/biological applications [10,11] namely as antifungal [12], antibacterial [13–15], anticancer [11,13,16,17], antiviral [18], as well as urease [19], XO [13], and helicase inhibitors [20]. Additionally, it has been established that this pyrimidine class of compounds undergoes Knoevenagel condensations with aldehydes to give 5-ylidene derivatives [13,21]. Furthermore, the formation of Michael adducts often follows Knoevenagel condensations with the formation of novel bis-thiobarbiturates [21]. On the other hand, bis-thiobarbiturates have been scarcely explored except that they have been established as urease inhibitors [22] and were tested as antibacterials but without any relevant activity [15].

2. Materials and Methods

2.1. Chemicals and Instrumentation

All reagents and solvents used were analytically pure and were used without purification. Ethanol was purchased from Honeywell (Paris, France), acetic acid from José M. Vaz Pereira, S. A. (Sintra, Portugal) and petroleum ether from Chem-Lab (Zedelgem, Belgium). Barbituric and 2-thiobarbituric acids and 2,4-dinitrobenzaldehyde were obtained from Alfa Aesar (Kandel, Germany), while 2-nitrobenzaldehyde was from Maybridge (Loughborough, United Kingdom). *N,N*-Diethyl-2-thiobarbituric acid, 4-formylbenzotrile, 4-methoxybenzaldehyde, 5-hydroxy-2-nitrobenzaldehyde, 6-nitrobenzo[*d*][1,3]dioxole-5-carbaldehyde and 3-pyridinecarboxaldehyde were acquire from Acros Organics (Geel, Belgium). Benzaldehyde, 4-methylbenzaldehyde, 4-nitrobenzaldehyde, *N*-(4-formylphenyl)acetamide, 4-bromobenzaldehyde, 3-hydroxybenzaldehyde, 4-(dimethylamino)-2-nitrobenzaldehyde and α -methyl-*trans*-cinnamaldehyde were obtained from Sigma-Aldrich (St. Louis, MO, USA).

All reactions were monitored by thin-layer chromatography on precoated silica-gel aluminum plates of 0.2 mm (Macherey-Nagel 60 G/UV254, Düren, Germany). After the elution, the plates' observation was performed under ultraviolet (UV) light with a wavelength of 254 and/or 365 nm.

The melting points (mp) were determined in open capillary tubes using a Büchi B-540 mp apparatus and were not corrected.

Proton (^1H NMR) and carbon nuclear magnetic resonance (^{13}C NMR) spectra were performed on a Bruker Avance III 400 MHz spectrophotometer and were processed by the software MestReNova 14.2.0 lite (Mestrelab Research S.L., Santiago de Compostela, Spain). Deuterated chloroform (CDCl_3 , Acros Organics, Geel, Belgium) or hexadeuterodimethyl sulfoxide ($\text{DMSO-}d_6$, Eurisotop, Gif-sur-Yvette, France) were used as a solvent and internal standard, $\delta = 7.26$ and 77.16 ppm or 2.50 and 39.52 ppm in ^1H and ^{13}C NMR, respectively. The chemical shift (δ) values are given in parts per million (ppm) and coupling constants (*J*) in Hertz (Hz). The multiplicity of the signals is reported as singlet (s), doublet (d), doublet of doublets (dd), doublet of triplets (dt), doublet of doublet of triplets (ddt), triplet (t), triplet of doublets (td), triplet of triplets (tt), quartet (q), quartet of doublets (qd), or multiplet (m).

High-resolution mass spectrometry (HRMS) was performed for new compounds by electrospray ionization time-of-flight (ESI-TOF) at CACTI services from the University of Vigo (Spain).

2.2. Synthesis of Bis-Thiobarbiturates 3–19

A mixture of barbituric acid **1c** or thiobarbituric acids **1a–b** (2.0 mmol) and a benzaldehyde **2a–m** or aldehydes **2n–o** (1.0 mmol) in ethanol (5 mL) was stirred for two to six hours, at room temperature (rt) or by reflux [22] or alternatively in acetic acid (5 mL) at 80 °C [23]. The obtained solid was filtered, washed with cold ethanol and petroleum ether 40–60 °C, dried, and recrystallized from ethanol to afford the following bis-barbiturate and bis-thiobarbiturates **3–19**.

5,5'-(Phenylmethylene)bis(1,3-diethyl-6-hydroxy-2-thioxo-2,3-dihydropyrimidin-4(1H)-one) (**3**)

From *N,N*-diethyl-2-thiobarbituric acid (**1a**, 2.0 mmol, 400.6 mg) and benzaldehyde (**2a**, 1.0 mmol, 106.1 mg, 101.6 μ L) in ethanol at rt; yellow solid (434.9 mg, 89% yield); mp: 177–179 °C; ^1H NMR (400 MHz, CDCl_3) δ (ppm) 7.32 (t, $J = 7.7$ Hz, 2H, 2 \times ArCH), 7.26 (t, $J = 7.4$ Hz, 1H, ArCH), 7.13 (d, $J = 7.9$ Hz, 2H, 2 \times ArCH), 5.68 (s, 1H, 5-CCH), 4.76–4.50 (m, 8H, 4 \times NCH₂CH₃), 1.38 (t, $J = 7.0$ Hz, 6H, 2 \times NCH₂CH₃), 1.29 (t, $J = 7.0$ Hz, 6H, 2 \times NCH₂CH₃); Figure S4. ^{13}C NMR (101 MHz, CDCl_3) δ (ppm) 174.71 (2 \times 2-CS), 163.84 (2 \times CO), 162.38 (2 \times CO), 135.62 (ArC), 128.58 (2 \times ArCH), 126.90 (ArCH), 126.43 (2 \times ArCH), 97.55 (2 \times 5-C), 45.26 (2 \times NCH₂CH₃), 44.70 (2 \times NCH₂CH₃), 35.03 (5-CCH), 12.20 (2 \times NCH₂CH₃), 12.12 (2 \times NCH₂CH₃); Figure S5.

5,5'-(*p*-Tolymethylene)bis(1,3-diethyl-6-hydroxy-2-thioxo-2,3-dihydropyrimidin-4(1H)-one) (**4**)

From *N,N*-diethyl-2-thiobarbituric acid (**1a**, 2.0 mmol, 400.6 mg) and 4-methylbenzaldehyde (**2b**, 1.0 mmol, 120.2 mg, 118.0 μ L) in ethanol at rt; yellow solid (397.1 mg, 79% yield); mp: 163–164 °C; ^1H NMR (400 MHz, CDCl_3) δ (ppm) 7.12 (d, $J = 8.1$ Hz, 2H, 2 \times ArCH), 7.00 (d, $J = 8.3$ Hz, 2H, 2 \times ArCH), 5.63 (s, 1H, 5-CCH), 4.91–4.47 (m, 8H, 4 \times NCH₂CH₃), 2.34 (s, 3H, ArCCH₃), 1.38 (t, $J = 7.0$ Hz, 6H, 2 \times NCH₂CH₃), 1.29 (t, $J = 7.0$ Hz, 6H, 2 \times NCH₂CH₃); Figure S6. ^{13}C NMR (101 MHz, CDCl_3) δ (ppm) 174.66 (2 \times 2-CS), 163.79 (2 \times CO), 162.34 (2 \times CO), 136.46 (ArC), 132.44 (ArC), 129.28 (2 \times ArCH), 126.29 (2 \times ArCH), 97.67 (2 \times 5-C), 45.23 (2 \times NCH₂CH₃), 44.65 (2 \times NCH₂CH₃), 34.71 (5-CCH), 21.09 (ArCCH₃), 12.19 (2 \times NCH₂CH₃), 12.11 (2 \times NCH₂CH₃); Figure S7.

4-(Bis(1,3-diethyl-6-hydroxy-4-oxo-2-thioxo-1,2,3,4-tetrahydropyrimidin-5-yl)methyl) benzonitrile (**5**)

From *N,N*-diethyl-2-thiobarbituric acid (**1a**, 2.0 mmol, 400.6 mg) and 4-formylbenzonitrile (**2c**, 1.0 mmol, 131.1 mg) in ethanol at rt; white solid (400.6 mg, 78% yield); mp: 199–200 °C; ^1H NMR (400 MHz, CDCl_3) δ (ppm) 7.62 (d, $J = 8.5$ Hz, 2H, 2 \times ArCH), 7.27 (d, $J = 8.5$ Hz, 2H, 2 \times ArCH), 5.66 (s, 1H, 5-CCH), 4.90–4.42 (m, 8H, 4 \times NCH₂CH₃), 1.37 (t, $J = 7.0$ Hz, 6H, 2 \times NCH₂CH₃), 1.28 (t, $J = 7.0$ Hz, 6H, 2 \times NCH₂CH₃); Figure S8. ^{13}C NMR (101 MHz, CDCl_3) δ (ppm) 174.71 (2 \times 2-CS), 163.93 (2 \times CO), 162.35 (2 \times CO), 141.76 (ArC), 132.40 (2 \times ArCH), 127.42 (2 \times ArCH), 118.74 (ArCCN), 110.92 (ArC), 96.73 (2 \times 5-C), 45.35 (2 \times NCH₂CH₃), 44.80 (2 \times NCH₂CH₃), 35.43 (5-CCH), 12.14 (2 \times NCH₂CH₃), 12.12 (2 \times NCH₂CH₃); Figure S9.

5,5'-(4-Nitrophenyl)methylene)bis(1,3-diethyl-6-hydroxy-2-thioxo-2,3-dihydropyrimidin-4(1H)-one) (**6**)

From *N,N*-diethyl-2-thiobarbituric acid (**1a**, 2.0 mmol, 400.6 mg) and 4-nitrobenzaldehyde (**2d**, 1.0 mmol, 151.1 mg) in ethanol at rt; yellow solid (416.2 mg, 78% yield); mp: 202–204 °C; ^1H NMR (400 MHz, CDCl_3) δ (ppm) 8.18 (d, $J = 8.9$ Hz, 2H, 2 \times ArCH), 7.33 (d, $J = 8.9$ Hz, 2H, 2 \times ArCH), 5.69 (s, 1H, 5-CCH), 4.77–4.38 (m, 8H, 4 \times NCH₂CH₃), 1.37 (t, $J = 7.0$ Hz, 6H, 2 \times NCH₂CH₃), 1.29 (t, $J = 7.0$ Hz, 6H, 2 \times NCH₂CH₃); Figure S10. ^{13}C NMR (101 MHz, CDCl_3) δ (ppm) 174.72 (2 \times 2-CS), 163.93 (2 \times CO), 162.39 (2 \times CO), 146.92 (ArC), 143.88 (ArC), 127.56 (2 \times ArCH), 123.82 (2 \times ArCH), 96.82 (2 \times 5-C), 45.38 (2 \times NCH₂CH₃), 44.82 (2 \times NCH₂CH₃), 35.43 (5-CCH), 12.14 (2 \times NCH₂CH₃), 12.12 (2 \times NCH₂CH₃); Figure S11.

5,5'-(4-Nitrophenyl)methylene)bis(6-hydroxy-2-thioxo-2,3-dihydropyrimidin-4(1H)-one) (**7**)

From 2-thiobarbituric acid (**1b**, 2.0 mmol, 258.6 mg) 4-nitrobenzaldehyde (**2d**) (1.0 mmol, 152.3 mg) in ethanol at reflux; pale yellow solid (303.5 mg; 72% yield); mp: 225 °C dec.; ¹H NMR (400 MHz, DMSO-*d*₆) δ (ppm) 11.76 (s, 4H, 4 × NH), 8.07 (d, *J* = 8.7 Hz, 2H, 2 × ArCH), 7.27 (d, *J* = 8.5 Hz, 2H, 2 × ArCH), 6.04 (s, 1H, 5-CCH); Figure S12. ¹³C NMR (101 MHz, DMSO-*d*₆) δ (ppm) 173.16 (2 × 2-CS), 163.04 (4 × CO), 151.99 (ArC), 145.34 (ArC), 127.88 (2 × ArCH), 123.16 (2 × ArCH), 95.28 (2 × 5-C), 31.29 (5-CCH); Figure S13.

5,5'-((4-Nitrophenyl)methylene)bis(6-hydroxypyrimidine-2,4(1H,3H)-dione) (**8**)

From barbituric acid (**1c**, 2.0 mmol, 231.8 mg) 4-nitrobenzaldehyde (**2d**) (1.0 mmol, 152.3 mg) in ethanol at reflux during six hours; white solid (319.2 mg, 82% yield); mp: 227 °C dec.; ¹H NMR (400 MHz, DMSO-*d*₆) δ (ppm) 10.74 (s, 4H, 4 × NH), 8.08 (d, *J* = 8.7 Hz, 2H, 2 × ArCH), 7.37 (d, *J* = 8.4 Hz, 2H, 2 × ArCH), 5.82 (s, 1H, 5-CCH); Figure S14. ¹³C NMR spectra was not herein present due to a rapid product decomposition in DMSO-*d*₆ solution.

N-(4-(Bis(1,3-diethyl-6-hydroxy-4-oxo-2-thioxo-1,2,3,4-tetrahydropyrimidin-5-yl)methyl)phenyl)acetamide (**9**)

From *N,N*-diethyl-2-thiobarbituric acid (**1a**, 2.0 mmol, 400.6 mg) and *N*-(4-formylphenyl)acetamide (**2e**, 1.0 mmol, 167.2 mg) in ethanol at rt; yellow solid (485.6 mg, 89% yield); mp: 178–179 °C; ¹H NMR (400 MHz, CDCl₃) δ (ppm) 7.47 (d, *J* = 8.3 Hz, 2H, 2 × ArCH), 7.17 (s, 1H, NHCOCH₃), 7.06 (d, *J* = 8.1 Hz, 2H, 2 × ArCH), 5.62 (s, 1H, 5-CCH), 4.74–4.52 (m, 8H, 4 × NCH₂CH₃), 2.17 (s, 3H, NHCOCH₃), 1.37 (t, *J* = 6.9 Hz, 6H, 2 × NCH₂CH₃), 1.28 (t, *J* = 7.0 Hz, 6H, 2 × NCH₂CH₃); Figure S15. ¹³C NMR (101 MHz, CDCl₃) δ (ppm) 174.47 (2 × 2-CS), 168.76 (NHCOCH₃), 163.59 (2 × CO), 162.13 (2 × CO), 137.25 (ArC), 130.59 (ArC), 126.72 (2 × ArCH), 119.64 (2 × ArCH), 97.40 (2 × 5-C), 45.06 (2 × NCH₂CH₃), 44.48 (2 × NCH₂CH₃), 34.45 (5-CCH), 24.37 (NHCOCH₃), 12.01 (2 × NCH₂CH₃), 11.95 (2 × NHCH₂CH₃); Figure S16. HMRS (ESI-TOF): *m/z* [M + H]⁺ calcd for C₂₅H₃₂N₅O₅S₂: 546.1839; found: 546.1840.

5,5'-((4-Methoxyphenyl)methylene)bis(1,3-diethyl-6-hydroxy-2-thioxo-2,3-dihydropyrimidin-4(1H)-one) (**10**)

From *N,N*-diethyl-2-thiobarbituric acid (**1a**, 2.0 mmol, 400.6 mg) and 4-methoxybenzaldehyde (**2f**, 1.0 mmol, 136.2 mg) in acetic acid at 80 °C; yellow solid (352.7 mg, 68% yield); mp: 139–140 °C; ¹H NMR (400 MHz, CDCl₃) δ (ppm) 7.02 (dd, *J* = 8.8, 1.0 Hz, 2H, 2 × ArCH), 6.84 (d, *J* = 8.8 Hz, 2H, 2 × ArCH), 5.62 (s, 1H, 5-CCH), 4.75–4.45 (m, 8H, 4 × NCH₂CH₃), 3.80 (s, 3H, OCH₃), 1.37 (t, *J* = 7.0 Hz, 6H, 2 × NCH₂CH₃), 1.29 (t, *J* = 7.0 Hz, 6H, 2 × NCH₂CH₃); Figure S17. ¹³C NMR (101 MHz, CDCl₃) δ (ppm) 174.67 (2 × 2-CS), 163.78 (2 × CO), 162.34 (2 × CO), 158.44 (ArC), 127.54 (2 × ArCH), 127.34 (ArC), 113.95 (2 × ArCH), 97.76 (2 × 5-C), 55.39 (OCH₃), 45.26 (2 × NCH₂CH₃), 44.69 (2 × NCH₂CH₃), 34.36 (5-CCH), 12.20 (2 × NCH₂CH₃), 12.14 (2 × NCH₂CH₃); Figure S18.

5,5'-((4-Bromophenyl)methylene)bis(1,3-diethyl-6-hydroxy-2-thioxo-2,3-dihydropyrimidin-4(1H)-one) (**11**)

From *N,N*-diethyl-2-thiobarbituric acid (**1a**, 2.0 mmol, 400.6 mg) and 4-bromobenzaldehyde (**2g**, 1.0 mmol, 185.0 mg) in ethanol at rt; white solid (402.9 mg, 64% yield); mp: 169–170 °C; ¹H NMR (400 MHz, CDCl₃) δ (ppm) 7.43 (dt, *J* = 8.6, 2.6, 1.9 Hz, 2H, 2 × ArCH), 7.01 (dt, *J* = 8.6, 2.7, 1.8 Hz, 2H, 2 × ArCH), 5.59 (s, 1H, 5-CCH), 4.81–4.45 (m, 8H, 4 × NCH₂CH₃), 1.37 (t, *J* = 7.0 Hz, 6H, 2 × NCH₂CH₃), 1.29 (t, *J* = 7.0 Hz, 6H, 2 × NCH₂CH₃); Figure S19. ¹³C NMR (101 MHz, CDCl₃) δ (ppm) 174.71 (2 × 2-CS), 163.87 (2 × CO), 162.33 (2 × CO), 134.91 (ArC), 131.66 (2 × ArCH), 128.33 (2 × ArCH), 120.79 (ArC), 97.19 (2 × 5-C), 45.31 (2 × NCH₂CH₃), 44.75 (2 × NCH₂CH₃), 34.78 (5-CCH), 12.18 (2 × NCH₂CH₃), 12.13 (2 × NCH₂CH₃); Figure S20.

5,5'-((3-Hydroxyphenyl)methylene)bis(1,3-diethyl-6-hydroxy-2-thioxo-2,3-dihydropyrimidin-4(1H)-one) (**12**)

From *N,N*-diethyl-2-thiobarbituric acid (**1a**, 2.0 mmol, 400.6 mg) and 3-hydroxybenzaldehyde (**2h**, 1.0 mmol, 123.9 mg) in ethanol at rt; yellow solid (183.9 mg, 73% yield); mp:

191–193 °C; ^1H NMR (400 MHz, CDCl_3) δ (ppm) 7.12 (t, $J = 7.9$ Hz, 1H, ArCH), 6.68 (ddt, $J = 8.0, 2.1, 1.0$ Hz, 1H, ArCH), 6.60 (dt, $J = 8.2, 1.9, 0.9$ Hz, 1H, ArCH), 6.58 (dd, $J = 2.1, 1.0$ Hz, 1H, ArCH), 5.57 (s, 1H, 5-CCH), 4.75–4.44 (m, 8H, 4 \times NCH₂CH₃), 1.34 (t, $J = 7.0$ Hz, 6H, 2 \times NCH₂CH₃), 1.26 (t, $J = 7.0$ Hz, 6H, 2 \times NCH₂CH₃); Figure S21. ^{13}C NMR (101 MHz, CDCl_3) δ (ppm) 174.58 (2 \times 2-CS), 163.61 (2 \times CO), 162.28 (2 \times CO), 157.36 (ArC), 137.22 (ArC), 129.35 (ArCH), 117.49 (ArCH), 113.93 (ArCH), 113.77 (ArCH), 97.52 (2 \times 5-C), 45.11 (2 \times NCH₂CH₃), 44.60 (2 \times NCH₂CH₃), 34.85 (5-CCH), 12.12 (2 \times NCH₂CH₃), 12.04 (2 \times NCH₂CH₃); Figure S22.

5,5'-((2-Nitrophenyl)methylene)bis(1,3-diethyl-6-hydroxy-2-thioxo-2,3-dihydropyrimidin-4(1H)-one) (13)

From *N,N*-diethyl-2-thiobarbituric acid (**1a**, 2.0 mmol, 400.6 mg) and 2-nitrobenzaldehyde (**2i**, 1.0 mmol, 151.1 mg) in ethanol at rt; rose solid (474.9 mg, 89% yield); mp: 172–173 °C; ^1H NMR (400 MHz, CDCl_3) δ (ppm) 7.56 (dd, $J = 7.8, 1.4$ Hz, 1H, ArCH), 7.52 (td, $J = 7.7, 1.5$ Hz, 1H, ArCH), 7.42 (tt, $J = 7.6, 1.1$ Hz, 1H, ArCH), 7.28 (dt, $J = 7.9, 1.1$ Hz, 1H, ArCH), 6.11 (s, 1H, 5-CCH), 4.63 (q, $J = 7.0$ Hz, 4H, 2 \times NCH₂CH₃), 4.59–4.47 (m, 4H, 2 \times NCH₂CH₃), 1.36 (t, $J = 7.0$ Hz, 6H, 2 \times NCH₂CH₃), 1.28 (t, $J = 7.0$ Hz, 6H, 2 \times NCH₂CH₃); Figure S23. ^{13}C NMR (101 MHz, CDCl_3) δ (ppm) 174.56 (2 \times 2-CS), 163.77 (2 \times CO), 162.15 (2 \times CO), 150.18 (ArC), 131.44 (ArCH), 129.64 (ArCH), 129.42 (ArC), 128.18 (ArCH), 124.24 (ArCH), 96.73 (2 \times 5-C), 45.22 (2 \times NCH₂CH₃), 44.73 (2 \times NCH₂CH₃), 32.75 (5-CCH), 12.04 (2 \times NCH₂CH₃), 11.87 (2 \times NCH₂CH₃); Figure S24.

5,5'-((4-(Dimethylamino)-2-nitrophenyl)methylene)bis(1,3-diethyl-6-hydroxy-2-thioxo-2,3-dihydropyrimidin-4(1H)-one) (14)

From *N,N*-diethyl-2-thiobarbituric acid (**1a**, 2.0 mmol, 400.6 mg) and 4-(dimethylamino)-2-nitrobenzaldehyde (**2j**, 1.0 mmol, 200.2 mg) in ethanol at rt; red solid (490.2 mg, 85% yield); mp: 143–145 °C; ^1H NMR (400 MHz, CDCl_3) δ (ppm) 7.10 (d, $J = 8.3$ Hz, 1H, ArCH), 7.06–6.96 (m, 2H, 2 \times ArCH), 6.01 (s, 1H, 5-CCH), 4.63 (q, $J = 7.1$ Hz, 4H, 2 \times NCH₂CH₃), 4.57–4.45 (m, 4H, 2 \times NCH₂CH₃), 3.03 (s, 6H, N(CH₃)₂), 1.36 (t, $J = 6.8$ Hz, 6H, 2 \times NCH₂CH₃), 1.29 (t, $J = 7.1$ Hz, 6H, 2 \times NCH₂CH₃); Figure S25. ^{13}C NMR (101 MHz, CDCl_3) δ (ppm) 174.54 (2 \times 2-CS), 163.71 (2 \times CO), 162.12 (2 \times CO), 150.87 (ArC), 147.87 (ArC), 130.62 (ArCH), 118.95 (ArC), 116.46 (ArCH), 109.51 (ArCH), 97.00 (2 \times 5-C), 45.22 (2 \times NCH₂CH₃), 44.72 (2 \times NCH₂CH₃), 41.78 (N(CH₃)₂), 32.12 (5-CCH), 12.08 (2 \times NCH₂CH₃), 11.94 (2 \times NCH₂CH₃); Figure S26. HMRS (ESI-TOF): m/z [M + H]⁺ calcd for C₂₅H₃₃N₆O₆S₂: 577.1898; found: 577.1891.

5,5'-((2,4-Dinitrophenyl)methylene)bis(1,3-diethyl-6-hydroxy-2-thioxo-2,3-dihydropyrimidin-4(1H)-one) (15)

From *N,N*-diethyl-2-thiobarbituric acid (**1a**, 2.0 mmol, 400.6 mg) and 2,4-dinitrobenzaldehyde (**2k**, 1.0 mmol, 196.1 mg) in ethanol at rt; yellow solid (434.0 mg, 75% yield); mp: 169–170 °C; ^1H NMR (400 MHz, CDCl_3) δ (ppm) 8.41 (d, $J = 2.3$ Hz, 1H, ArCH), 8.37 (dd, $J = 8.7, 2.4$ Hz, 1H, ArCH), 7.52 (dd, $J = 8.7, 1.3$ Hz, 1H, ArCH), 6.11 (s, 1H, 5-CCH), 4.63 (q, $J = 7.0$ Hz, 4H, 2 \times NCH₂CH₃), 4.59–4.46 (m, 4H, 2 \times NCH₂CH₃), 1.37 (t, $J = 7.0$ Hz, 6H, 2 \times NCH₂CH₃), 1.29 (t, $J = 7.0$ Hz, 6H, 2 \times NCH₂CH₃); Figure S27. ^{13}C NMR (101 MHz, CDCl_3) δ (ppm) 174.57 (2 \times 2-CS), 163.85 (2 \times CO), 162.21 (2 \times CO), 149.93 (ArC), 146.87 (ArC), 137.06 (ArC), 131.25 (ArCH), 125.67 (ArCH), 119.58 (ArCH), 95.99 (2 \times 5-C), 45.34 (2 \times NCH₂CH₃), 44.87 (2 \times NCH₂CH₃), 33.34 (5-CCH), 12.01 (2 \times NCH₂CH₃), 11.89 (2 \times NCH₂CH₃); Figure S28.

5,5'-((5-Hydroxy-2-nitrophenyl)methylene)bis(1,3-diethyl-6-hydroxy-2-thioxo-2,3-dihydropyrimidin-4(1H)-one) (16)

From *N,N*-diethyl-2-thiobarbituric acid (**1a**, 2.0 mmol, 400.6 mg) and 5-hydroxy-2-nitrobenzaldehyde (**2l**, 1.0 mmol, 167.1 mg) in ethanol at rt; yellow solid (505.7 mg, 92% yield); mp: 167–169 °C; ^1H NMR (400 MHz, CDCl_3) δ (ppm) 7.53 (d, $J = 8.6$ Hz, 1H, ArCH), 6.74 (dd, $J = 8.6, 2.5$ Hz, 1H, ArCH), 6.70 (d, $J = 2.2$ Hz, 1H, ArCH), 6.10 (s, 1H, 5-CCH), 4.58 (q, $J = 7.0$ Hz, 4H, 2 \times NCH₂CH₃), 4.49 (m, 4H, 2 \times NCH₂CH₃), 1.31 (t, $J = 7.0$ Hz, 6H, 2 \times NCH₂CH₃), 1.22 (t, $J = 6.9$ Hz, 6H, 2 \times NCH₂CH₃); Figure S29. ^{13}C NMR (101 MHz,

CDCl₃) δ (ppm) 174.35 (2 \times 2-C_S), 163.51 (2 \times C=O), 161.86 (2 \times C=O), 160.76 (ArC), 141.96 (ArC), 132.45 (ArC), 127.17 (ArCH), 116.99 (ArCH), 113.93 (ArCH), 97.01 (2 \times 5-C), 45.04 (2 \times NCH₂CH₃), 44.60 (2 \times NCH₂CH₃), 33.01 (5-CCH), 11.96 (2 \times NCH₂CH₃), 11.76 (2 \times NCH₂CH₃); Figure S30. HMRS (ESI-TOF): m/z [M + H]⁺ calcd for C₂₃H₂₈N₅O₇S₂: 550.1425; found: 550.1417.

5,5'-((6-Nitrobenzo[*d*][1,3]dioxol-5-yl)methylene)bis(1,3-diethyl-6-hydroxy-2-thioxo-2,3-dihydropyrimidin-4(1H)-one) (17)

From *N,N*-diethyl-2-thiobarbituric acid (**1a**, 2.0 mmol, 400.6 mg) and 6-nitrobenzo[*d*]dioxole-5-carbaldehyde (**2m**, 1.0 mmol, 199.1 mg) in ethanol at rt; yellow solid (429.4 mg, 77% yield); mp: 148–149 °C; ¹H NMR (400 MHz, CDCl₃) δ (ppm) 7.11 (s, 1H, ArCH), 6.67 (d, *J* = 1.1 Hz, 1H, ArCH), 6.11 (s, 2H, OCH₂O), 6.10 (d, *J* = 1.1 Hz, 1H, 5-CCH), 4.68–4.46 (m, 8H, 4 \times NCH₂CH₃), 1.36 (t, *J* = 7.0 Hz, 6H, 2 \times NCH₂CH₃), 1.28 (t, *J* = 7.0 Hz, 6H, 2 \times NCH₂CH₃); Figure S31. ¹³C NMR (101 MHz, CDCl₃) δ (ppm) 174.50 (2 \times 2-C_S), 163.79 (2 \times C=O), 162.06 (2 \times C=O), 150.44 (ArC), 146.72 (ArC), 144.08 (ArC), 125.75 (ArC), 109.24 (OCH₂O), 105.84 (ArCH), 103.09 (ArCH), 97.06 (2 \times 5-C), 45.24 (2 \times NCH₂CH₃), 44.73 (2 \times NCH₂CH₃), 32.83 (5-CCH), 12.03 (2 \times NCH₂CH₃), 11.88 (2 \times NCH₂CH₃); Figure S32. HMRS (ESI-TOF): m/z [M + H]⁺ calcd for C₂₄H₂₈N₅O₈S₂: 578.1374; found: 578.1381.

5,5'-(2-Methyl-3-phenylprop-2-ene-1,1-diyl)bis(1,3-diethyl-6-hydroxy-2-thioxo-2,3-dihydropyrimidin-4(1H)-one) (18)

From *N,N*-diethyl-2-thiobarbituric acid (**1a**, 2.0 mmol, 400.6 mg) and α -methyl-*trans*-cinnamaldehyde (**2n**, 1.0 mmol, 150.5 mg, 145.1 μ L) in ethanol at rt; yellow solid (264.3 mg, 50% yield); mp: 145–146 °C; ¹H NMR (400 MHz, CDCl₃) δ (ppm) 7.34 (t, *J* = 7.8 Hz, 2H, 2 \times ArCH), 7.25–7.19 (m, 3H, 3 \times ArCH), 6.27 (s, 1H, 5-CCH), 5.01 (q, *J* = 2.7, 1.4 Hz, 1H, C=CH), 4.77–4.51 (m, 8H, 4 \times NCH₂CH₃), 1.77 (t, *J* = 1.3 Hz, 3H, CCH₃), 1.36 (t, *J* = 7.0 Hz, 6H, 2 \times NCH₂CH₃), 1.31 (t, *J* = 7.0 Hz, 6H, 2 \times NCH₂CH₃); Figure S33. ¹³C NMR (101 MHz, CDCl₃) δ (ppm) 174.62 (2 \times 2-C_S), 163.61 (2 \times C=O), 162.39 (2 \times C=O), 138.02 (ArC), 131.24 (C=CH), 129.04 (2 \times ArCH), 128.26 (2 \times ArCH), 126.72 (ArCH), 126.60 (C=CH), 97.53 (2 \times 5-C), 45.26 (2 \times NCH₂CH₃), 44.72 (2 \times NCH₂CH₃), 38.27 (5-CCH), 17.19 (CCH₃), 12.19 (2 \times NCH₂CH₃), 12.15 (2 \times NCH₂CH₃); Figure S34. HMRS (ESI-TOF): m/z [M + H]⁺ calcd for C₂₆H₃₃N₄O₄S₂: 529.1938; found: 529.1939.

5,5'-(Pyridin-3-ylmethylene)bis(1,3-diethyl-6-hydroxy-2-thioxo-2,3-dihydropyrimidin-4(1H)-one) (19)

From *N,N*-diethyl-2-thiobarbituric acid (**1a**, 2.0 mmol, 400.6 mg) and 3-pyridinecarboxaldehyde (**2o**, 1.0 mmol, 109.3 mg, 95.9 μ L) in ethanol at rt; yellow solid (264.4 mg, 54% yield); mp: 253–254 °C; ¹H NMR (400 MHz, DMSO-*d*₆) δ (ppm) 8.69 (d, *J* = 5.6 Hz, 1H, ArCH), 8.58 (s, 1H, ArCH), 8.27 (d, *J* = 8.2 Hz, 1H, ArCH), 7.92 (dd, *J* = 8.2, 5.5 Hz, 1H, ArCH), 6.43 (s, 1H, 5-CCH), 4.44 (qd, *J* = 13.0, 6.4 Hz, 8H, 4 \times NCH₂CH₃), 1.17 (t, *J* = 6.8 Hz, 12H, 4 \times NCH₂CH₃); Figure S35. ¹³C NMR (101 MHz, DMSO-*d*₆) δ (ppm) 174.65 (2 \times 2-C_S), 161.13 (4 \times C=O), 144.71 (ArCH), 143.15 (ArC), 140.14 (ArCH), 139.24 (ArCH), 126.70 (ArCH), 94.24 (2 \times 5-C), 43.12 (4 \times NCH₂CH₃), 32.24 (5-CCH), 12.30 (4 \times NCH₂CH₃); Figure S36.

2.3. In Vitro Studies

XO inhibitory and antioxidant assays were performed in triplicate while antiproliferative assay was conducted in quadruplicate. For each assay, at least two independent experiments were performed. An initial screening at the concentration of 30 μ M for all compounds under study was performed in each in vitro study. A second screening at 5 μ M was performed for compounds that originated an inhibitory potential higher than 80% for the XO activity at 30 μ M. Half-maximal inhibitory concentration (IC₅₀) studies were performed for drugs used as a reference and for the most promising bis-thiobarbiturate in XO inhibitory, antioxidant, and cytotoxicity assays.

2.3.1. Solutions Preparation

For in vitro studies, all bis-thiobarbiturates, Allo, febuxostat, Trolox, and 5-fluorouracil (5-FU) were dissolved in DMSO at the concentration of 10 mM. Additionally, a 10 mM xanthine solution was prepared in a 25 mM sodium hydroxide solution. All solutions were kept at a temperature of 4 °C before each experiment. Allo, febuxostat, Trolox, and 5-FU were purchased from Sigma-Aldrich (St. Louis, MO, USA).

2.3.2. XO Inhibitory Assay

The XO inhibitory activity was evaluated by spectrophotometric quantification of uric acid formation [13]. The 50 mM dihydrogen phosphate buffer (pH 7.4) was used to dilute all solutions. For each assay performed, 50 µL of the test solution and 50 µL of the 0.1 U/mL XO (Sigma-Aldrich X4875, St. Louis, MO, USA) solution were added in each well of an Elisa microplate (96 wells) followed by 5 min of incubation at 37 °C. Final concentrations of 50, 25, 10, 5, 1, and 0.5 µM for Allo, 0.5, 0.075, 0.05, 0.025, 0.01, and 0.001 µM for febuxostat and 10, 5, 2.5, 1, 0.5, and 0.1 µM for bis-thiobarbiturate **11** were used for IC₅₀ determinations. The reaction started with the addition of 150 µL of a xanthine solution (420 µM). The absorbance was recorded at a wavelength of 295 nm every minute for 10 min. To obtain only the absorbance associated with uric acid, a solution consisting of 50 µL of the test solution, 150 µL of the xanthine solution, and 50 µL of buffer were used as blank. Additionally, the dihydrogen phosphate buffer was used as a negative control and Allo and febuxostat as positive controls. For each compound, the percentage of enzyme inhibition was calculated according to the following formula:

$$\% \text{ of XO inhibition} = [1 - (\text{ABS}_{\text{sample}} - \text{ABS}_{\text{blank of sample}}) / \text{ABS}_{\text{negative control}}] \times 100$$

2.3.3. Antioxidant Assay

Antioxidant potential was spectrophotometrically evaluated by the 2,2-diphenyl-1-picrylhydrazyl (DPPH, Sigma-Aldrich, St. Louis, MO, USA) method [13]. All solutions and dilutions were prepared in 99.5% ethanol before each experiment. For each assay, 100 µL of the test solution and 100 µL of DPPH solution (0.2 mM) were added to each well of a 96 wells Elisa microplate. Final concentrations of 120, 60, 30, 15, 7.5, 3.75, and 1 µM for Trolox and bis-thiobarbiturate **11** were used for IC₅₀ determinations. After 60 min of incubation in dark at rt, the capacity of each compound to reduce DPPH was followed by measuring the absorbance at 517 nm. Ethanol was used as a negative control and Trolox as the positive control. To discount the absorbance of each compound at 517 nm, a blank was performed with 100 µL of each test compound and 100 µL of ethanol. The antioxidant capacity of each sample was calculated according to the following formula:

$$\% \text{ DPPH scavenging} = [1 - (\text{ABS}_{\text{sample}} - \text{ABS}_{\text{blank of sample}}) / \text{ABS}_{\text{negative control}}] \times 100$$

2.3.4. Cytotoxicity Assay

The cytotoxic potential of the compounds being studied was evaluated by quantifying the extent of the reduction of 3-(4,5-dimethylthiazol-2-yl)-2,5-diphenyltetrazolium bromide (MTT, VWR, Radnor, PA, USA) [24] on tumor cell lines of the colon (Caco-2) and breast (MCF-7) adenocarcinoma and non-tumor human dermal fibroblasts (NHDF). All cell lines were obtained from the American Type Culture Collection (ATCC, Manassas, VA, USA) and were maintained in 75 cm² culture flasks in a humidified air incubator with 5% CO₂ at 37 °C. NHDF cells have grown in RPMI 1640 medium (Sigma-Aldrich, St. Louis, MO, USA) supplemented with 10% fetal bovine serum (FBS), 10 mM 4-(2-hydroxyethyl)-1-piperazineethanesulfonic acid (HEPES), 2 mM L-glutamine, 1 mM sodium pyruvate, and 1% antibiotic/antimycotic (Ab: 10,000 units/mL penicillin G, 100 mg/mL streptomycin and 25 µg/mL amphotericin B). MCF-7 cells were cultured in high-glucose Dulbecco's modified Eagle medium (DMEM, Sigma-Aldrich, St. Louis, MO, USA) supplemented with 10% FBS, and 1% Ab. The Caco-2 cell line was cultured in a high glucose DMEM supplemented with

20% FBS and 1% of the antibiotic mixture (Sp: 10,000 units/mL penicillin G and 100 mg/mL of streptomycin). For the assay, cells were seeded in 96-well plates (2×10^4 cells/mL) in the culture medium. After 48 h of adherence, cells were treated with the test solutions and incubated for 72 h. Final concentrations of 200, 100, 50, 10, 1, and 0.1 μ M for bis-thiobarbiturate **11** were used for IC₅₀ determinations. Untreated cells were used as a negative control and 5-FU as the positive control. Following incubation, the medium was removed and replaced with a fresh incomplete culture medium (without FBS and Ab or Sp) and MTT solution [5 mg/mL in phosphate buffer saline (PBS)]. After further incubation for 4 h at 37 °C, the medium with MTT was removed, formazan crystals were dissolved in DMSO, and the absorbance was read at 570 nm. Results were expressed as the relative cell proliferation in comparison with the negative control cells.

2.3.5. Statistics

All in vitro results are expressed as mean values \pm standard deviation (SD) of at least two independent determinations. The difference between groups was analyzed for each assay by Student's *t*-test. The IC₅₀ values were calculated by sigmoidal fitting analysis considering a 95% confidence interval.

2.4. In Silico Studies

Drug-likeness of bis-thiobarbiturate **11** was verified by the free web tool SwissADME [25]. Absorption, distribution, metabolism, excretion, and toxicity (ADMET) parameters were evaluated at SwissADME [25] and pkCSM [26] web tools.

3. Results and Discussion

Bis-diethylthiobarbiturates **3–6**, **9**, and **11–19** were synthesized by the method previously described [22]; although, and to the best of our knowledge, compounds **9**, **14**, **16–18** have never been described in the literature. These conditions are characterized by a short reaction time and simplicity of reaction conditions, affording the desired products with a high degree of purity even without crystallization. Furthermore, this method was carried out at rt, and the product was easily isolated by filtration, in moderate to excellent reactional yields, from 50 to 92% (Table 1). Bis-diethylthiobarbiturate **10**, bis-thiobarbiturate **7**, and bis-barbiturate **8** were synthesized by modified processes once the conditions used at rt were not successfully in affording the respective arylidene. Thus, bis-diethylthiobarbiturate **10** was synthesized in acetic acid at 80 °C [23], and bis-(thio)barbiturates **7–8** were synthesized in ethanol at reflux temperature. The formation of bis-(thio)barbiturates **3–19** was confirmed by NMR, since a singlet in the range of 5.58 to 6.43 ppm and a signal from 31.3 to 38.3 ppm in ¹H and ¹³C NMR spectra, respectively, were obtained for the aryltrisubstituted methyne group. On the other hand, when arylidene derivatives were formed, a singlet at 8 ppm in ¹H NMR and 153 ppm in ¹³C NMR were observed [13]. Despite the synthesis and isolation of bis-barbiturate **8**, a DMSO-*d*₆ solution rapid decomposition to the barbituric acid (**1c**) and respective arylidene was observed (Scheme S1), in accordance with the literature [27]. Therefore, bis-barbiturate **8** was not used in further biological studies.

The XO inhibitory assay of the synthesized bis-thiobarbiturates was performed by a spectrophotometric method at 295 nm, and commercial febuxostat and Allo were used as positive controls. The study started with a screening at the concentration of 30 μ M, and all sixteen bis-thiobarbiturates demonstrated potential as XO inhibitors (Figure 1 and Table S1), with inhibitions from 14.92 to 95.72% (88.51% for Allo and 95.03% for febuxostat). After this study, an additional screening at 5 μ M was performed for the target compounds that presented an inhibition higher than 80% at 30 μ M. Thus, the identification of the most promising bis-thiobarbiturates under study for further concentration-response studies was performed.

In order to perform some structure-activity relationships inferences, firstly the influence of *N* substitution in the thiobarbituric acid moiety was analyzed. Results demonstrated that *N* substitution with ethyl group at thiobarbiturate moiety led to an increment in XO

inhibitory activity from 20.86 to 92.25% (7 versus 6). Taking both results in mind, several bis-diethylthiobarbiturates with different substituent groups mainly at *para* position of phenyl moiety were analyzed in detail. In this context, electron-withdrawing groups appear to intensify the XO inhibitory potential in relation to electron-donating counterparts. In fact, the presence of nitrile, nitro, or bromo groups at *para* position increases the inhibitory activity from 80.15% (unsubstituted 3) to 86.12, 92.25, and 95.72% at 30 μ M, and from 10.42% to 52.92, 56.82, and 80.92% at 5 μ M, for 5, 6, and 11, respectively. On the other hand, the addition of a methyl, acetamide or methoxy group at the same position reduces the inhibitory activity to 36.47, 45.61, and 23.53 at 30 μ M, for 4, 9, and 10 respectively. Besides these effects observed for different groups in the *para* position, a small decrease in the inhibitory activity was observed when the same group was in the *ortho* position. This effect is notoriously noticed for the bis-thiobarbiturates *para*-nitro and *ortho*-nitro substituted pair, where the values of XO inhibitions are 56.82 and 37.42% at 5 μ M, for 6 and 13, respectively.

Table 1. Chemical synthesis, structure and reactional yields of bis-(thio)barbiturates 3–19.

Bis-(thio) Barbiturate	Starting Material	X	R ₁	R ₂	R ₃	Yield (%)
3	1a + 2a	S	Et	H	-	89
4	1a + 2b	S	Et	4-CH ₃	-	79
5	1a + 2c	S	Et	4-CN	-	78
6	1a + 2d	S	Et	4-NO ₂	-	78
7	1b + 2d	S	H	4-NO ₂	-	72
8	1c + 2d	O	H	4-NO ₂	-	82
9	1a + 2e	S	Et	4-NHCOCH ₃	-	89
10	1a + 2f	S	Et	4-OCH ₃	-	68
11	1a + 2g	S	Et	4-Br	-	71
12	1a + 2h	S	Et	3-OH	-	73
13	1a + 2i	S	Et	2-NO ₂	-	78
14	1a + 2j	S	Et	2-NO ₂ , 4-N(CH ₃) ₂	-	85
15	1a + 2k	S	Et	2,4-NO ₂	-	75
16	1a + 2l	S	Et	2-NO ₂ , 5-OH	-	92
17	1a + 2m	S	Et	2-NO ₂ , 4,5-OCH ₂ O	-	77
18	1a + 2n	S	Et	-		50
19	1a + 2o	S	Et	-		54

The analysis of the influence of the presence of di and tri substitutions in phenyl moiety on the percentage of XO inhibition seems not to be straightforward. Indeed, the additional presence of a dimethylamine group at the *para* position or two methylenedioxy groups at the *meta* and *para* positions of the *ortho*-nitro group substituted seems to increase the XO inhibitory activity at 5 μ M (14 and 17 versus 13). However, the additional presence of a *para*-nitro or *meta*-hydroxyl decreases the XO inhibitory activity (15 and 16 versus 13). A deeply notorious reduction of XO inhibitory activity at 30 μ M was observed with

a double nitro substitution (14.92%; **15**) concerning the related *ortho*- (89.73%; **13**) or *para*- (92.25%; **6**) mono-nitro congener. Additionally, this effect was also noted for the bis-thiobarbiturates **12** (72.25%; 3-hydroxyl) and **13** (89.73%; 2-nitro) when compared with their related bis-thiobarbiturates **16** (61.44%; 2-nitro, 5-hydroxyl).

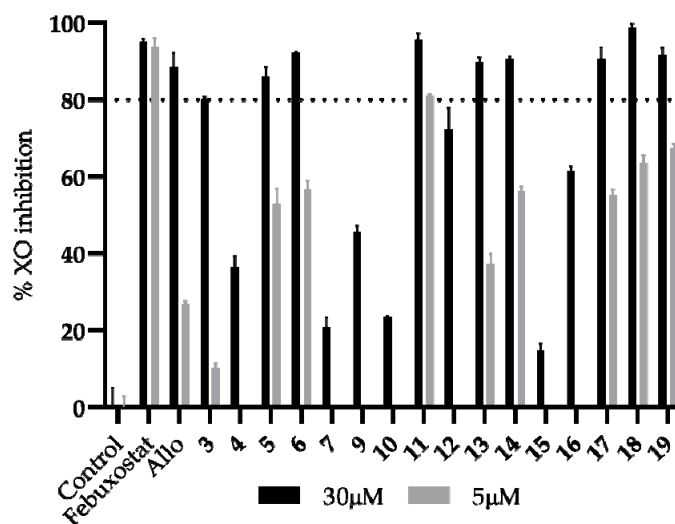


Figure 1. In vitro XO inhibitory activity of bis-thiobarbiturates 3–7 and 9–19 and references febuxostat and Allo. Results are expressed as average values \pm SD of two independent determinations, and each one was performed in triplicate. A $p < 0.01$ versus the negative control in the statistical significance analysis (Student's *t*-test) was observed for all compounds.

Finally, the replacement of the phenyl (bis-thiobarbiturate **3**) moiety for 2-methyl-3-phenylprop-2-enyl or pyridin-3-yl showed a promising increment for activity at 5 μ M by about six-fold (**3** versus **18** and **19**).

In conclusion, bis-thiobarbiturates **5**, **6**, **11**, **13**, **14**, **17**, **18**, and **19** evidence a percentage of XO inhibition higher than Allo at 5 μ M; however, this is still lower than the second positive control, febuxostat. Generally, the most active compounds present electron-withdrawing or halogen substituents on the phenyl ring. Nevertheless, the effect of further electron-withdrawing and/or electron-donating group substitutions must be carefully balanced.

The halogenated bis-thiobarbiturate **11** demonstrated that it was the most promising within this set of tested compounds. Further concentration-response studies for **11** showed the inhibition of XO was activity-dependent on the concentration, presenting a calculated IC_{50} value of 1.79 μ M (Table 2 and Figure S1), being approximately ten-fold more active than the positive control Allo (IC_{50} of 10.73 μ M), one of the reference drugs used for gout treatment.

Table 2. In vitro IC_{50} values (μ M) for XO inhibition, DPPH radical scavenging activity and cytotoxicity on NHDF cell line of bis-thiobarbiturate **11** and respective references Allo and Trolox ^a.

	XO Inhibition		DPPH Scavenging		Cytotoxicity on NHDF	
	IC_{50}	R^2	IC_{50}	R^2	IC_{50}	R^2
Febuxostat	0.03 ± 0.01	0.9732	n.d. ^b	-	n.d. ^b	-
Allo	10.73 ± 0.81	0.9959	n.d. ^b	-	n.d. ^b	-
Trolox	n.d. ^b	-	23.82 ± 2.13	0.9947	n.d. ^b	-
11	1.79 ± 0.07	0.9986	24.67 ± 0.88	0.9992	93.15 ± 5.54	0.8913

^a IC_{50} value \pm SD represents as mean at least two independent determinations. ^b n.d. is not determined.

Since both steps of XO purine catabolism led to ROS generation (Scheme S2), a dual effect as an XO inhibitor and antioxidant can be profitable for new antigout drugs, since ROS generated by XO can produce cytotoxic effects in many circumstances and thus can promote mutagenesis and tumor development [3]. Therefore, molecules capable of this dual XO inhibitory and radical scavenging activity could be even more advantageous for gout treatment.

The antioxidant potential of all synthesized bis-thiobarbiturates 3–7 and 9–19 was evaluated by the DPPH method at a concentration of 30 μM , and results were compared with a reference compound, Trolox. The analysis of results (Figure 2 and Table S1) showed the high antioxidant potential of tested 3–7 and 9–18. The only exception was 19 that shows a low DPPH scavenging activity. Withal, the weak antioxidant activity of Allo was also evidenced, as expected [14]. Although a modest influence of several substituents on DPPH scavenging activity at 30 μM was noticed, some interesting conclusions can be inferred. Aligned with XO inhibitory results, the most DPPH scavenging bis-thiobarbiturate is once again the halogenated derivative 11. In fact, the IC_{50} value determined for 11 is similar to that obtained for Trolox (24.67 and 23.82 μM , respectively) in DPPH radical scavenging activity concentration-response studies (Table 2 and Figure S2).

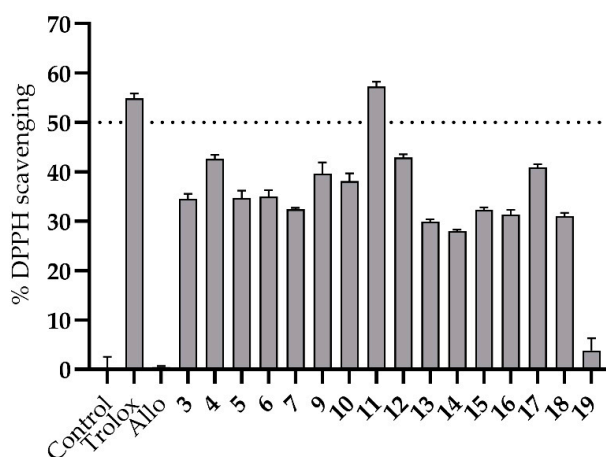


Figure 2. In vitro DPPH radical scavenging activity of bis-thiobarbiturates 3–7 and 9–19, Allo and reference Trolox. Results are expressed as average values \pm SD of two independent determinations, and each one was performed in triplicated. A $p < 0.001$ versus the negative control in the statistical significance analysis (Student's t -test) was observed for all compounds except for Allo and 19.

Regarding the promising results of the bis-thiobarbiturate 11 on both antioxidant and XO inhibitory activity, the in vitro biosafety effectiveness was further analyzed by the MTT method in a non-tumoral cell line. A calculated IC_{50} of 93.15 μM (Table 2 and Figure S3) clearly demonstrated the low cytotoxicity of this compound on NHDF cells at concentrations where XO inhibitory activity was effective. Thus, despite being used in vitro data, it was possible to calculate the selectivity index for bis-thiobarbiturate 11, with calculated values of 52.04 and 3.77 for XO inhibition and DPPH scavenging activity, respectively.

Although there is no direct relationship between the use of XO inhibitors and a good prognosis in cancer treatment, the expression and activity of this enzyme have been negatively associated with a high degree of malignancy and a worse prognosis in some types of cancer, namely of the breast and gastrointestinal tract, in recent years [28,29]. Considering the low cytotoxicity on NHDF cells observed for bis-thiobarbiturate 11, the interest of barbiturate and thiobarbiturate derivatives as anticancer agents [11,13] and the recent work on XO inhibitors with anticancer activity [30], we decided to evaluate the cytotoxicity on NHDF as well as the antiproliferative effects on colorectal adenocarcinoma Caco-2 and breast cancer MCF-7 cell lines for all bis-thiobarbiturates under study. To get a

strengthened term of comparison, the anticancer drug 5-FU was used as a positive control. From the results (Figure 3 and Table S1), the not-marked cytotoxicity of almost all tested compounds was noted. In fact, only bis-thiobarbiturates **10**, **13**, **16**, and **17** demonstrated a relevant effect on NHDF cells, with cell viability below 80%. On the other hand, all of the tested bis-thiobarbiturates did not present antiproliferative effects on the breast cancer MCF-7 cell line. Nonetheless, on the colorectal Caco-2 cancer cell line, bis-thiobarbiturates **5**, **9**, **10**, and **11** showed a moderate effect on their cell viability; however, it was weaker than the positive control 5-FU. In addition, compounds **5**, **9**, and **11** demonstrated some selectivity for cancer Caco-2 *versus* normal NHDF cells.

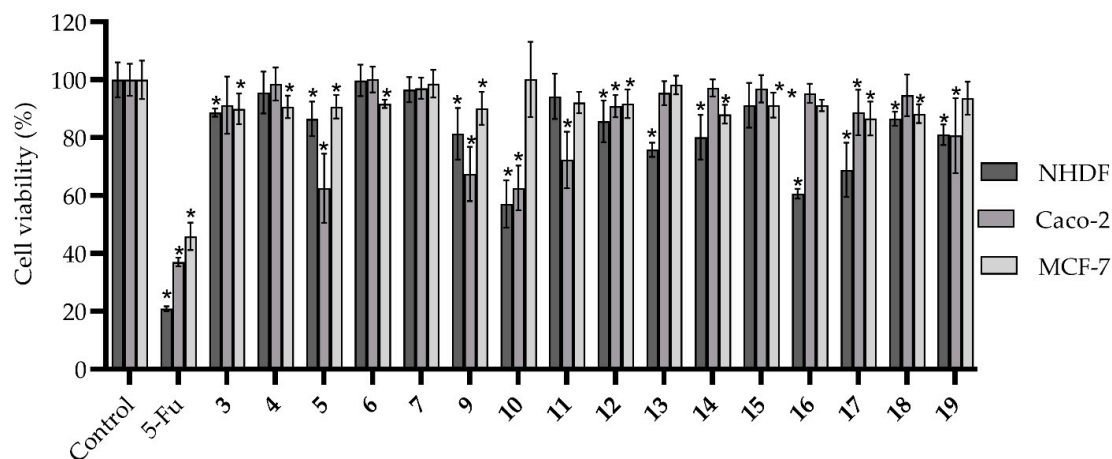


Figure 3. In vitro effects of bis-thiobarbiturates 3–7 and 9–19 and 5-FU on cell viability of non-tumor cell lines of normal human dermal fibroblasts (NHDF), and human adenocarcinoma tumor cell lines of colorectal (Caco-2) and breast (MCF-7), at the single concentration of 30 μ M. Results are expressed as average values \pm standard deviation of at least two independent assays performed in quadruplicate. * $p < 0.05$ versus the negative control by Student's *t*-test.

In silico approaches remain a critical tool for drug discovery since their use can be a determinant for a cost-effective identification of promising drug candidates and to reduce the use of animal models [31,32]. In this context, the most promising *bis*-thiobarbiturate herein tested, **11**, was in silico assessed to verify its drug-likeness characteristics with the applicability of Lipinski's rule of five [33] and Veber's parameters [34] by the free web tool SwissADME [25]. These two rules are essential tools in drug discovery to predict the potential bioavailability of new drug candidates. Therefore, it was determined that compound **11** respect Lipinski's rule parameters for hydrogen bond donors (nOHNH), hydrogen bond acceptors (nON) and octanol-water partition coefficient (logP) (Table 3). The exception to this rule was only a molecular weight larger than 500. However, this is not a preponderant factor, since it has been considered that one violation of this rule is acceptable [33]. The alternative analysis of the variant of Lipinski's rule of five by Veber et al. even claims that a molecular weight cutoff at 500 by itself does not suggest compounds with low bioavailability. Veber's parameters defend a simple analysis of the number of rotatable bonds (n-rot; 10 or fewer) and topological polar surface area (TPSA; equal to or less than 140 \AA^2 or 12 or fewer nON and nOHNH) [34]. Taking this consideration in mind leads us to conclude that *bis*-thiobarbiturate **11** has a high probability of presenting good bioavailability. Despite presenting TPSA superior to 140 \AA^2 , *bis*-thiobarbiturate **11** does not exceed the allowed number of nON and nOHNH.

Table 3. In silico molecular properties of bis-thiobarbiturate **11** using the SwissADME predictive database ^a.

Descriptor		Value
Molecular weight		567.52 g/mol
Log P		4.01
nON		6
nOHNH		2
n-rot		7
TPSA		158.50 Å ²
Drug-likeness	Lipinski	Yes; 1 violation: MW > 500
	Veber	Yes
Medicinal Chemistry	PAINS	0 alert

^a Octanol-water partition coefficient (logP); number of hydrogen bond acceptors (nON); number of hydrogen bond donors (nOHNH); number of rotatable bonds (n-rot); topological polar surface area (TPSA); Lipinski's rule of five: molecular weight < 500 Da; logP < 5; n-OHNH < 5; n-OHNH < 10. A maximum of 1 violation is permitted [33]. Veber's parameters: n-rot ≤ 10; TPSA ≤ 140 Å² or total of nON and nOHNH ≤ 12 [34].

The identification of **11** as a potential promiscuous compound with reactivity on several biological targets [35] was also crucial for their potential interest in medicinal chemistry. The results obtained eliminate the potential of **11** to be a pan-assay interference compound (PAINS), since no significant alerts were observed. Although some barbituric and thiobarbituric acid derivatives are considered to be highly reactive with numerous biological targets [35], the hypothesis of the *bis*-thiobarbiturate **11** as PAINS is thus removed.

The ADMET parameters of the *bis*-thiobarbituric **11** were then evaluated on SwissADME [25] and pkCSM [26] web tools. As expected from the fulfillment of Lipinski's and Veber's rules, **11** presents potentially good intestinal absorption (71.66%) with moderate solubility in water (Table 4). In addition, compound **11** should not be a potential substrate for P-glycoprotein, an important parameter to consider in the study of drug-drug interactions [36]. Besides, interactions with organic cation transporter 2 (OCT2) [36] and cytochrome P450 (CYP) enzymes [37] are two other important checks to take in mind. In accordance and as expected, **11** reveals not to be a substrate for renal OCT2 CYP1A2, CYP2C19, and CYP2D6 inhibitors. On the other hand, **11** could likely be a potential inhibitor for CYP2C9 and CYP3A4.

Table 4. In silico pharmacokinetic (absorption, distribution, metabolism, and excretion) and toxicity parameters of bis-thiobarbiturate **11** using pkCSM and SwissADME predictive databases ^a.

Property	Model Name	Predicted Value
Absorption	Water solubility	−4.66 ^b (Moderately soluble)
	Intestinal absorption (human)	71.66%
	P-glycoprotein substrate	No
Distribution	BBB permeant	No
	LogBB	−1.38
	LogPS	−2.42
Metabolism	CYP1A2 inhibitor	No
	CYP2C19 inhibitor	No
	CYP2C9 inhibitor	Yes
	CYP2D6 inhibitor	No
Excretion	CYP3A4 inhibitor	Yes
	Log total clearance	−0.36 ^c
	Renal OCT2 substrate	No
Toxicity	AMES toxicity	No
	hERG I inhibitor	No
	hERG II inhibitor	No
	Hepatotoxicity	Yes
	Skin Sensitisation	No

^a Blood-brain barrier (BBB); logarithm of permeability in blood-brain barrier (logBB) < −1 are poorly distributed; blood-brain permeability-surface area product (logPS) > −2 are considered to penetrate the central nervous system and logPS < −3 are considered as unable to penetrate the central nervous system [26]; human ether-a-go-go-related gene (hERG). ^b log(mol/L). ^c log(mL/min/kg).

As barbiturate derivatives are potential CNS depressants [10], **11**'s distribution profile is additionally analyzed. In this context, *in silico* SwissADME predictions showed no expectable ability for **11** to permeate the blood-brain barrier (BBB). This low potential capacity of **11** to reach the CNS is corroborated by pkCSM calculated values of log BBB and log CNS.

Besides **11**'s low cytotoxicity on NHDF cells previously established, predictions by pkCSM indicated that their manipulation should not cause skin sensitization. This *bis*-thiobarbiturate also would not be genotoxic or cardiotoxic since it does not have the potential to originate human ether-a-go-go-related gene's (hERG's) inhibition. Nonetheless, **11** can be a potential hepatotoxic compound and future studies will be necessary to evaluate their *in vitro* and/or *in vivo* toxicity profile.

4. Conclusions

Bis-barbiturates and bis-thiobarbiturates were easily and straightforwardly synthesized in moderate to excellent reactional yields. These bis-thiobarbiturates stood out by their antioxidant performance and excellent ability to inhibit the XO at a concentration of 30 μ M. The most powerful bis-diethylthiobarbiturate within this set showed an XO inhibition IC₅₀ of 1.79 μ M, which was about ten-fold better than *in vitro* Allo inhibition, together with high DPPH radical scavenging activity and suitable low cytotoxicity. The *in silico* molecular properties such as druglikeness, pharmacokinetics and toxicity were fulfilled for this promising barbiturate, clearly pointing to the potential use of this class of molecules for the treatment of hyperuricemia diseases, such as gout.

5. Patents

"Bis-pirimidinonas como inibidores da xantina oxidase para o tratamento de condições patológicas causadas por hiperuricemia" PT116062 (20 January 2020).

Supplementary Materials: The following are available online at <https://www.mdpi.com/article/10.3390/biomedicines9101443/s1>, Table S1: Full *in vitro* data, Scheme S1: Chemical mechanism for the formation of bis-thiobarbiturates; Scheme S2: Diagram of XO oxidative hydroxylation's; Figures S1–S3: Curves for IC₅₀ calculations; Figures S4–S36: ¹H and ¹³C NMR spectra.

Author Contributions: Synthesis, J.L.S., D.L. and M.J.A.R.; XO inhibition studies and writing—original draft preparation, J.L.S. and D.L.; DPPH, Cytotoxic and *in silico* assays, J.L.S.; funding acquisition and writing—review and editing, R.E.F.B., S.S. and P.A.; supervision, S.S. and P.A. All authors have read and agreed to the published version of the manuscript.

Funding: This work is supported by funds from the Health Sciences Research Center (CICS-UBI) (UID/Multi/00709/2019) through National Funds by Fundação para a Ciência e Tecnologia (FCT). FEDER funds also support this work through the POCI-COMPETE 2020-Operational Programme Competitiveness and Internationalization in Axis I—Strengthening research, technological development and innovation [Programa Operacional Competitividade e Internacionalização (COMPETE 2020), project No. 007491]. It is also acknowledged funding from C4—Cloud Computing Competences Center project (CENTRO-01-0145-FEDER-000019). J. L. Serrano acknowledges a doctoral fellowship grant from FCT (SFRH/BD/148028/2019).

Institutional Review Board Statement: Not applicable.

Informed Consent Statement: Not applicable.

Conflicts of Interest: The authors declare that they have no knowledge of conflict of interest.

References

1. Šmelcerović, A.; Tomović, K.; Šmelcerović, Ž.; Petronijević, Ž.; Kocić, G.; Tomašić, T.; Jakopin, Ž.; Anderluh, M. Xanthine oxidase inhibitors beyond allopurinol and febuxostat; an overview and selection of potential leads based on *in silico* calculated physico-chemical properties, predicted pharmacokinetics and toxicity. *Eur. J. Med. Chem.* **2017**, *135*, 491–516. [CrossRef]
2. Cos, P.; Ying, L.; Calomme, M.; Hu, J.P.; Cimanga, K.; Van Poel, B.; Pieters, L.; Vlietinck, A.J.; Berghe, D.V. Structure–activity relationship and classification of flavonoids as inhibitors of xanthine oxidase and superoxide scavengers. *J. Nat. Prod.* **1998**, *61*, 71–76. [CrossRef]

3. Battelli, M.G.; Polito, L.; Bortolotti, M.; Bolognesi, A. Xanthine oxidoreductase-derived reactive species: Physiological and pathological effects. *Oxid. Med. Cell. Longev.* **2016**, *2016*, 3527579. [[CrossRef](#)] [[PubMed](#)]
4. Dalbeth, N.; Merriman, T.R.; Stamp, L.K. Gout. *Lancet* **2016**, *388*, 2039–2052. [[CrossRef](#)]
5. Martillo, M.A.; Nazzal, L.; Crittenden, D.B. The crystallization of monosodium urate. *Curr. Rheumat. Rep.* **2013**, *16*, 400. [[CrossRef](#)]
6. Benn, C.L.; Dua, P.; Gurrell, R.; Loudon, P.; Pike, A.; Storer, R.I.; Vangjeli, C. Physiology of hyperuricemia and urate-lowering treatments. *Front. Med.* **2018**, *5*, 160. [[CrossRef](#)]
7. Serrano, J.L.; Figueiredo, J.; Almeida, P.; Silvestre, S. From xanthine oxidase inhibition to in vivo hypouricemic effect: An integrated overview of in vitro and in vivo studies with focus on natural molecules and analogues. *Evid-Based. Complement. Alternat. Med.* **2020**, *2020*, 9531725. [[CrossRef](#)]
8. Singh, J.V.; Bedi, P.M.S.; Singh, H.; Sharma, S. Xanthine oxidase inhibitors: Patent landscape and clinical development (2015–2020). *Expert Opin. Ther. Pat.* **2020**, *30*, 769–780. [[CrossRef](#)]
9. Kerru, N.; Gummidi, L.; Maddila, S.; Gangu, K.K.; Jonnalagadda, S.B. A review on recent advances in nitrogen-containing molecules and their biological applications. *Molecules* **2020**, *25*, 1909. [[CrossRef](#)]
10. Nusrat, S.; Uzma, A.; Gul, Z.; Shagufta, P.; Irum, J.; Aisha, A. A comprehensive review: Bio-potential of barbituric acid and its analogues. *Curr. Org. Chem.* **2020**, *24*, 129–161.
11. Prasher, P.; Sharma, M.; Singh, S.P.; Rawat, D.S. Barbiturate derivatives for managing multifaceted oncogenic pathways: A mini review. *Drug Develop. Res.* **2021**, *82*, 364–373. [[CrossRef](#)]
12. Shabeer, M.; Barbosa, L.C.A.; Karak, M.; Coelho, A.C.S.; Takahashi, J.A. Thiobarbiturates as potential antifungal agents to control human infections caused by *Candida* and *Cryptococcus* species. *Med. Chem. Res.* **2018**, *27*, 1043–1049. [[CrossRef](#)]
13. Figueiredo, J.; Serrano, J.L.; Cavalheiro, E.; Keurulainen, L.; Yli-Kauhala, J.; Moreira, V.M.; Ferreira, S.; Domingues, F.C.; Silvestre, S.; Almeida, P. Trisubstituted barbiturates and thiobarbiturates: Synthesis and biological evaluation as xanthine oxidase inhibitors, antioxidants, antibacterial and anti-proliferative agents. *Eur. J. Med. Chem.* **2018**, *143*, 829–842. [[CrossRef](#)] [[PubMed](#)]
14. Figueiredo, J.; Serrano, J.L.; Soares, M.; Ferreira, S.; Domingues, F.C.; Almeida, P.; Silvestre, S. 5-Hydrazinylethylidene-pyrimidines effective against multidrug-resistant *Acinetobacter baumannii*: Synthesis and in vitro biological evaluation of antibacterial, radical scavenging and cytotoxic activities. *Eur. J. Pharm. Sci.* **2019**, *137*, 104964. [[CrossRef](#)]
15. Sharma, A.; Noki, S.; Zamisa, S.J.; Hazzah, H.A.; Almarhoon, Z.M.; El-Faham, A.; de la Torre, B.G.; Albericio, F. Exploiting the thiobarbituric acid scaffold for antibacterial activity. *ChemMedChem* **2018**, *13*, 1923–1930. [[CrossRef](#)]
16. Ortega, J.A.; Riccardi, L.; Minniti, E.; Borgogno, M.; Arencibia, J.M.; Greco, M.L.; Minarini, A.; Sissi, C.; De Vivo, M. Pharmacophore hybridization to discover novel topoisomerase II poisons with promising antiproliferative activity. *J. Med. Chem.* **2018**, *61*, 1375–1379. [[CrossRef](#)]
17. Bhatt, P.; Kumar, M.; Jha, A. Design, synthesis and anticancer evaluation of oxa/thiadiazolylhydrazones of barbituric and thiobarbituric acid: A collective in vitro and in silico approach. *ChemistrySelect* **2018**, *3*, 7060–7065. [[CrossRef](#)]
18. Cagno, V.; Tintori, C.; Civra, A.; Cavalli, R.; Tiberi, M.; Botta, L.; Brai, A.; Poli, G.; Tapparel, C.; Lembo, D.; et al. Novel broad spectrum virucidal molecules against enveloped viruses. *PLoS ONE* **2018**, *13*, e0208333.
19. Rauf, A.; Shahzad, S.; Bajda, M.; Yar, M.; Ahmed, F.; Hussain, N.; Akhtar, M.N.; Khan, A.; Jończyk, J. Design and synthesis of new barbituric- and thiobarbituric acid derivatives as potent urease inhibitors: Structure activity relationship and molecular modeling studies. *Bioorg. Med. Chem.* **2015**, *23*, 6049–6058. [[CrossRef](#)]
20. Marecki, J.C.; Aarattuthodiyl, S.; Byrd, A.K.; Penthalala, N.R.; Crooks, P.A.; Raney, K.D. N-Naphthoyl-substituted indole thiobarbituric acid analogs inhibit the helicase activity of the hepatitis C virus NS3. *Bioorg. Med. Chem. Lett.* **2019**, *29*, 430–434. [[CrossRef](#)]
21. Adamson, J.; Coe, J.B.; Grassam, L.H.; Jeffery, C.J.; Coles, J.S.; Hursthouse, B.M. Reactions of 1,3-diethyl-2-thiobarbituric acid with aldehydes: Formation of arylbis(1,3-diethyl-2-thiobarbitur-5-yl)methanes † and crystallographic evidence for ground state polarisation in 1,3-diethyl-5-[4-(dimethylamino)benzylidene]-2-thiobarbituric acid. *J. Chem. Soc. Perkin Trans. I* **1999**, *1*, 2483–2488. [[CrossRef](#)]
22. Rahim, F.; Ali, M.; Ullah, S.; Rashid, U.; Ullah, H.; Taha, M.; Javed, M.T.; Rehman, W.; Khan, A.A.; Abid, O.U.R.; et al. Development of bis-thiobarbiturates as successful urease inhibitors and their molecular modeling studies. *Chin. Chem. Lett.* **2016**, *27*, 693–697. [[CrossRef](#)]
23. Sachar, A.; Gupta, P.; Gupta, S.; Sharma, R.L. A novel approach towards the synthesis of tricyclic systems based on pyridine, pyran, thiopyran, azepine, oxepin, thiepin, and pyrimidine rings under different solvent conditions. *Can. J. Chem.* **2010**, *88*, 478–484. [[CrossRef](#)]
24. Matias, M.; Campos, G.; Santos, A.O.; Falcão, A.; Silvestre, S.; Alves, G. Potential antitumoral 3,4-dihydropyrimidin-2-(1H)-ones: Synthesis, in vitro biological evaluation and QSAR studies. *RSC Adv.* **2016**, *6*, 84943–84958. [[CrossRef](#)]
25. Daina, A.; Michielin, O.; Zoete, V. SwissADME: A free web tool to evaluate pharmacokinetics, drug-likeness and medicinal chemistry friendliness of small molecules. *Sci. Rep.* **2017**, *7*, 42717. [[CrossRef](#)]
26. Pires, D.E.V.; Blundell, T.L.; Ascher, D.B. pkCSM: Predicting small-molecule pharmacokinetic and toxicity properties using graph-based signatures. *J. Med. Chem.* **2015**, *58*, 4066–4072. [[CrossRef](#)]
27. Jursic, B.S.; Neumann, D.M. Preparation of 5,5'-pyridylidene and 5,5'-quinolidene bis-barbituric acid derivatives. *J. Het. Chem.* **2003**, *40*, 465–474. [[CrossRef](#)]

28. Battelli, M.G.; Bortolotti, M.; Polito, L.; Bolognesi, A. Metabolic syndrome and cancer risk: The role of xanthine oxidoreductase. *Redox Biol.* **2019**, *21*, 101070. [[CrossRef](#)]
29. Battelli, M.G.; Polito, L.; Bortolotti, M.; Bolognesi, A. Xanthine oxidoreductase in cancer: More than a differentiation marker. *Cancer Med.* **2016**, *5*, 546–557. [[CrossRef](#)]
30. Joshi, G.; Sharma, M.; Kalra, S.; Gavande, N.S.; Singh, S.; Kumar, R. Design, synthesis, biological evaluation of 3,5-diaryl-4,5-dihydro-1H-pyrazole carbaldehydes as non-purine xanthine oxidase inhibitors: Tracing the anticancer mechanism via xanthine oxidase inhibition. *Bioorg. Chem.* **2021**, *107*, 104620. [[CrossRef](#)]
31. Brogi, S.; Ramalho, T.C.; Kuca, K.; Medina-Franco, J.L.; Valko, M. Editorial: In silico methods for drug design and discovery. *Front. Chem.* **2020**, *8*, 612. [[CrossRef](#)] [[PubMed](#)]
32. Rifaioğlu, A.S.; Atas, H.; Martin, M.J.; Cetin-Atalay, R.; Atalay, V.; Doğan, T. Recent applications of deep learning and machine intelligence on in silico drug discovery: Methods, tools and databases. *Brief. Bioinform.* **2019**, *20*, 1878–1912. [[CrossRef](#)] [[PubMed](#)]
33. Lipinski, C.A.; Lombardo, F.; Dominy, B.W.; Feeney, P.J. Experimental and computational approaches to estimate solubility and permeability in drug discovery and development settings. *Adv. Drug Deliv. Rev.* **1997**, *23*, 3–25. [[CrossRef](#)]
34. Veber, D.F.; Johnson, S.R.; Cheng, H.-Y.; Smith, B.R.; Ward, K.W.; Kopple, K.D. Molecular properties that influence the oral bioavailability of drug candidates. *J. Med. Chem.* **2002**, *45*, 2615–2623. [[CrossRef](#)] [[PubMed](#)]
35. Baell, J.B.; Holloway, G.A. New substructure filters for removal of pan assay interference compounds (PAINS) from screening libraries and for their exclusion in bioassays. *J. Med. Chem.* **2010**, *53*, 2719–2740. [[CrossRef](#)]
36. Gessner, A.; König, J.; Fromm, M.F. Clinical aspects of transporter-mediated drug–drug interactions. *Clin. Pharmacol. Ther.* **2019**, *105*, 1386–1394. [[CrossRef](#)] [[PubMed](#)]
37. Manikandan, P.; Nagini, S. Cytochrome P450 structure, function and clinical significance: A review. *Curr. Drug Targets* **2018**, *19*, 38–54. [[CrossRef](#)] [[PubMed](#)]